JOURNAL OF MATERIALS SCIENCE 19 (1984) 3097–3106

Microstructure and mechanical properties of rapidly quenched $L2_0$ and $L2_0 + L1_2$ alloys in Ni–Al–Fe and Ni–Al–Co systems

A. INOUE, T. MASUMOTO
The Research Institute for Iron, Steel and Other Metals, Tohoku University, Sendai 980, Japan

H. TOMIOKA
Unitika Research and Development Center, Unitika Ltd, Uji 611, Japan

Ductile $L2_0$-type β' wires and $\beta' + L1_2$-type γ' duplex wires with high strengths and large elongation in the Ni–Al–Fe and Ni–Al–Co ternary systems have been manufactured directly from the liquid state by an in-rotating-water spinning method. The wire diameter was in the range 80 to 180 μm and the average grain size was $\sim$ 2 to 4 μm for the β' wires and $\sim$ 0.2 to 1.0 μm for the $\gamma' + \beta'$ wires. σ_y, σ_f and ϵ_p of the β' wires were found to be about 360 to 760 MPa, 560 to 960 MPa, and 0.2 to 5.5%, respectively, for the Ni–Al–Fe system, those of the $\gamma' + \beta'$ wires were about 395 to 660 MPa, 670 to 1285 MPa, and 3.5 to 17%, respectively, for the Ni–Al–Fe system, and about 260 to 365 MPa, 600 to 870 MPa, and 4.0 to 7.0%, respectively, for the Ni–Al–Co system. Cold-drawing caused a significant increase in σ_y and σ_f and the values attained were about 1850 and 2500 MPa, respectively, for Ni–20Al–30Fe and Ni–25Al–30Co wires drawn to about 90% reduction in area. The high strengths, large elongation and good cold-workability of the melt-quenched β' and $\gamma' + \beta'$ compound wires have been inferred to be due to the structural change into a low-degree ordered state containing a high density of phase boundaries, suppression of grain-boundary segregation and refinement of grain size.

1. Introduction

In recent years, metallic materials controlled structurally by melt-quenching techniques have attracted increasing interest because the melt-quenched alloys have a non-equilibrium structure, which is not obtained by the conventional fabricating process, and they exhibit various useful physical and chemical as well as good mechanical properties. In recent years, we have carried out a systematic investigation into quenching effect on the microstructure, mechanical strength and physical and chemical properties of iron- [1–8] and manganese-based [9] alloys which have an allotropic transformation, and for iron-based [10] and nickel-based [11] alloys which have an ordered structure up to the melting temperature, and have found that suppression of the allotropic transformation from austenite (γ) to ferrite (α) or martensite (α') etc, and of the development of an ordered structure, result in a drastic change from the extremely brittle nature in the usual solidified state to a ductile nature in the melt-quenched state. For instance, in ordered alloys, Inoue *et al.* have demonstrated that the melt-quenched $L1_2$-Ni_3Al (γ') compound in the Ni–Al–X (X = Cr, Mn, Fe, Co or Si) systems exhibits high strength combined with good ductility because of the structural change to a low degree of ordered state containing a high density of anti-phase boundaries (APB) and the suppression of grain-boundary segregation. A similar quenching effect is expected to occur for the $L2_0$ NiAl(β') compound and there is a high possibility that the melt-quenched β' compound will exhibit good ductility as well as high strength,

0022–2461/84 $03.00 + .12

even though the usually prepared β' compound is extremely brittle. The extreme brittleness is probably caused because the development of an ionic bonding nature associated with a strong ordered structure occurs between constituent atoms [12]. To our knowledge, no-one has succeeded to date in obtaining a ductile β' compound by any technique even such as thermomechanical treatment and impurity addition. The purpose of this paper is to examine the microstructure and mechanical properties of melt-quenched β' single phase and $\beta' + \gamma'$ duplex phases in Ni–Al–Fe and Ni–Al–Co systems and to investigate the quenching effect on the strength and ductility of the β' and $\beta' + \gamma'$ compounds.

2. Experimental methods

The specimens used in the present work were Ni–Al–Fe and Ni–Al–Co ternary alloys. All the compositions of these alloys are located in the formation regions of a β' single compound and the duplex compounds consisting of β' and γ'. The equilibrium phase diagrams [13–15] indicate that one chemical formula of the resultant compounds is (Ni–Fe)(Al–Fe) and $(Ni–Fe)_3(Al–Fe)$ for the Ni–Al–Fe system and (Ni–Co)(Al–Co) and $(Ni–Co)_3Al$ for the Ni–Al–Co system. Mixtures of the pure elements (Ni, Al and Fe or Co) were melted under an argon atmosphere in an induction furnace to prepare the test alloys. The melts were put into quartz tubes about 6 mm i.d. and solidifed in the tubes. Since the difference between weighed and chemically analysed compositions was less than 0.25 wt% for aluminium, the compositions are from the weighed values denoted by atomic percentage. From these master alloys, long ribbons with a cross-section of about 3 mm × 100 μm were prepared as the test samples for the structural observation by a melt-spinning apparatus. The amount of alloy melted in each run was about 3 g, and the rotation speed of the copper roller (200 mm diameter) was controlled to ~ 800 to 1000 r.p.m. In addition, continuous wires of ~ 80 to 180 μm diameter were prepared as samples for measuring mechanical properties using the in-rotating-water melt-spinning technique [16, 17] which is capable of producing wires with a circular cross-section directly from the molten metal. The main operating parameters for the production of continuous wires were adjusted as follows:

1. the distance between the surface of the water and the end of a quartz tube was less than about 3 mm and the angle of the nozzle against the water surface was about 70°;

2. the orifice size of the quartz nozzles varied from ~ 0.08 to 0.2 mm diameter;

3. the circumferential speed of the drum was approximately 10 to 13 m sec^{-1} and the melt jet velocity was lower by about 20 to 30% than that of the drum velocity;

4. the temperature of the cooling water was approximately 278 K; and

5. the melt was ejected by an argon over-pressure of about 0.2 MPa at a temperature of about 75 to 100 K above the liquidus.

The as-quenched and annealed structures of the specimen were examined by optical microscopy, transmission electron microscopy (TEM), and X-ray diffraction using filtered Cu$K\alpha$ radiation. The optical microscope samples were chemically polished in a solution of 96 parts ethyl alcohol and 4 parts nitric acid at room temperature, and the average grain size was determined from the optical micrographs of longitudinal and cross-sectional area. The TEM specimens were prepared by electrolytically thinning ribbons in a 1:9 volumetric ratio of perchloric acid methanol solution immersed in ice water. The yield strength (σ_y), tensile fracture strength (σ_f), and elongation (ϵ_p) were measured for the wire samples in as-quenched and 1 h annealed states at room temperature by an Instron-type tensile testing machine at a strain rate of 4.2×10^{-4} sec^{-1}. Tensile specimens were cut from an as-quenched long wire into short pieces having a gauge dimension of 20 mm length. A specially designed set of grips for the fine wires was used to ensure proper specimen alignment within the machine. The fracture surface morphology was examined using scanning electron microscopy.

3. Results

3.1. Microstructure of melt-quenched β' and $\beta' + \gamma'$ compounds

Fig. 1 shows the as-quenched structure and the corresponding selected-area diffraction patterns of melt-quenched Ni–20 at% Al–30 at% Fe (Ni–20Al–30Fe) alloy. The as-quenched structure is composed of duplex phases having a grain size as small as ~ 0.2 μm. Figs. 1b and c are the diffraction patterns in which the crystallographic normal is $[1\,1\,0]_{fcc}$ and $[1\,0\,0]_{bcc}$, respectively. In these patterns, small superlattice spots of 1 0 0 and 1 1 0

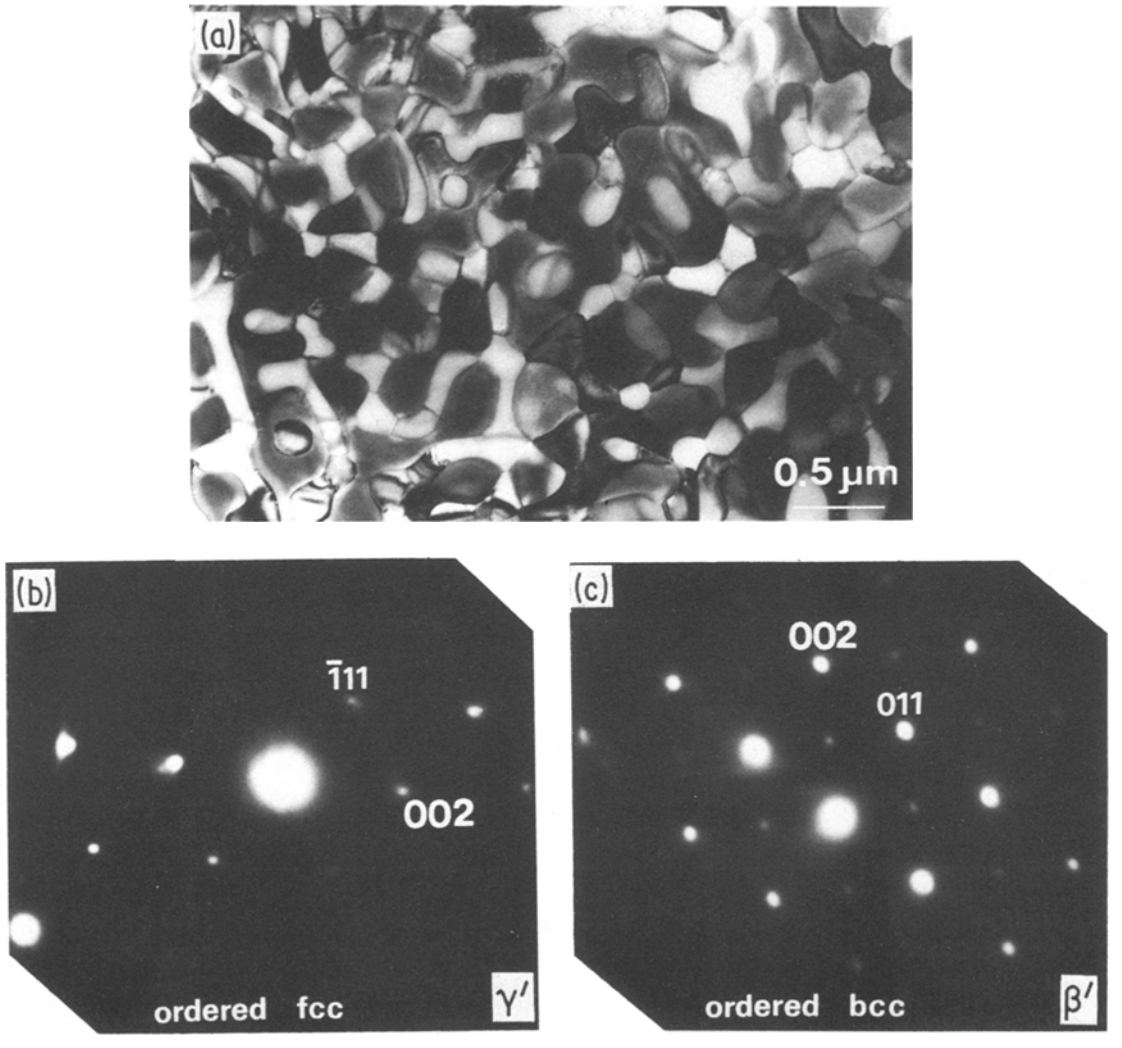

Figure 1 Transmission electron micrograph and selected-area diffraction patterns showing the melt-quenched structure of the Ni–20Al–30Fe alloy.

etc, are clearly seen besides the spots from the fundamental lattice. Analysis of these spots shows that the duplex phases consist of Ni_3Al (γ') with an ordered f c c structure and NiAl (β') with an ordered b c c structure. Judging from the composition of this alloy and the equilibrium phase diagram of Ni–Al–Fe ternary alloy [13, 14], the chemical formulae of these phases seem to be $(Ni, Fe)_3(Al, Fe)$ and (Ni, Fe)(Al, Fe). Fig. 2 shows the β' single phase and its selected-area diffraction pattern of melt-quenched Ni–30Al–20Fe alloy. No second phase is seen even on the grain boundaries. Thus, further increase in aluminium content results in the structural change from the duplex $\gamma' + \beta'$ phases to the β' single phase accompanied by a significant coarsening of grain size from about 0.2 μm to 4 μm.

A similar duplex structure consisting of γ' and β' phases is also formed in the Ni–25Al–40Co alloy, as shown in Fig. 3. The average grain size of the γ' and β' phases is different, being about 0.15 μm for the γ' phase and 0.5 μm for the β' phase.

3.2. Mechanical properties

First the morphology of the wires which were fabricated under the conditions described in Section 2 and used for measuring mechanical properties are reported. Fig. 4, for example, shows an optical micrograph of the cross-section of an

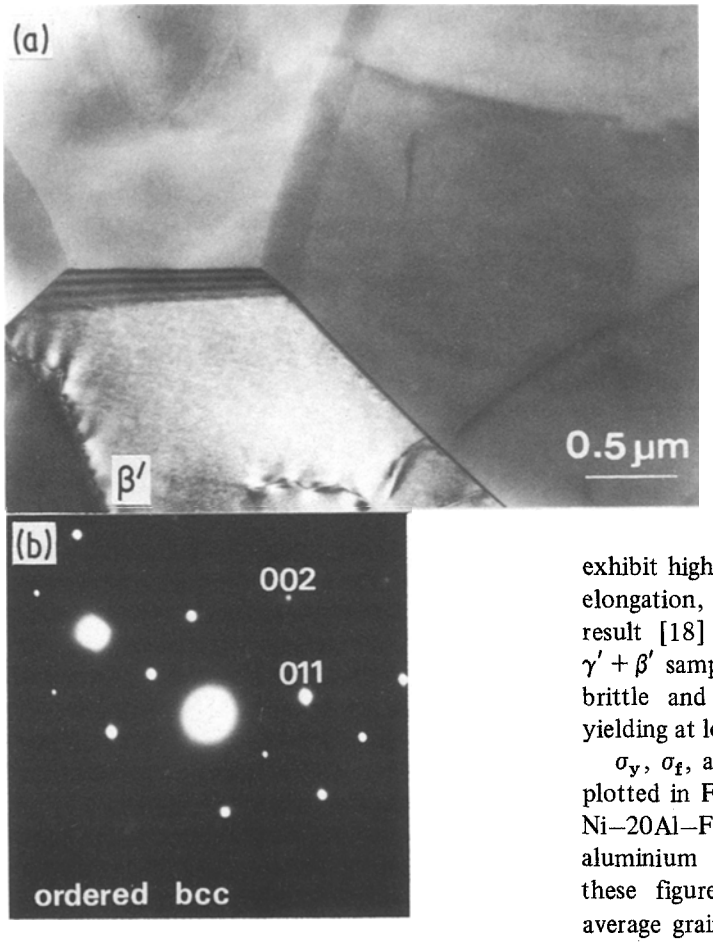

Figure 2 Transmission electron micrograph and selected-area diffraction pattern showing the melt-quenched structure of the Ni–30Al–20Fe alloy.

Ni–20Al–30Fe wire having the duplex structure of $\gamma' + \beta'$. It can be seen that the wire has an almost completely circular cross-section whose diameter is about 95 μm. Fig. 5 shows the typical examples of uniaxial tensile stress–elongation curves of the $\gamma' + \beta'$ and β' wires in Ni–Al–Fe system. The behaviour depends strongly on the melt-quenched structure:

1. the Ni–20Al–30Fe alloy having the $\gamma' + \beta'$ duplex structure exhibits high values of σ_y and σ_f and an elongation (ϵ_p) as large as ~ 17%;

2. the Ni–30Al–20Fe alloy having the β' single phase, in which no developed modulated structure is observed, exhibits low values of σ_y and σ_f and a relatively large ϵ_p of about 5%;

3. the Ni–30Al–30Fe alloy in which the β' single phase has a developed modulated structure exhibits an extremely low value of ϵ_p, even though σ_y is higher than those of the former two alloys.

It should be emphasized in Fig. 5 that the $\gamma' + \beta'$ and β' wires in the Ni–Al–Fe system exhibit high tensile strengths combined with large elongation, in good contrast to the previous result [18] that conventionally solidified β' and $\gamma' + \beta'$ samples in the alloy system are extremely brittle and undergo fracture immediately after yielding at low stresses.

σ_y, σ_f, and ϵ_p of the $\gamma' + \beta'$ and β' wires are plotted in Fig. 6 as a function of iron content for Ni–20Al–Fe alloys and in Fig. 7 as a function of aluminium content for Ni–Al–30Fe alloys. In these figures, the melt-quenched structure and average grain size are also shown for comparison. σ_y increases gradually from 400 MPa for the $\gamma' + \beta'$ wires to 725 MPa for the β' wires with increasing iron or aluminium content, but no appreciable deflection phenomenon in the compositional dependence of σ_y is detected around the phase boundary of $\gamma' + \beta'$ to β'. σ_f increases from 670 to 1285 MPa with increasing iron content (i.e. increasing volume fraction of β' phase) in the range of $\gamma' + \beta'$ duplex phases, whereas in the range of β' single phase, σ_f decreases significantly from 960 to 560 MPa with increasing iron or aluminium content. Judging from the result that the compositional dependence of σ_f is analogous to that of ϵ_p, the decrease in σ_f is concluded to be due to the decrease in the work-hardening amount caused by the decrease in ductility. The significant decrease in ductility with increasing iron or aluminium content is considered to be closely related to an enhancement of the phase separation of β'(Ni, Fe)(Al, Fe) compound into NiAl-rich and Fe-rich phases. Evidence for this is shown in Fig. 8 where the modulated contrast along the $\{1\,0\,0\}_{\beta'}$ plane becomes clearer with increasing

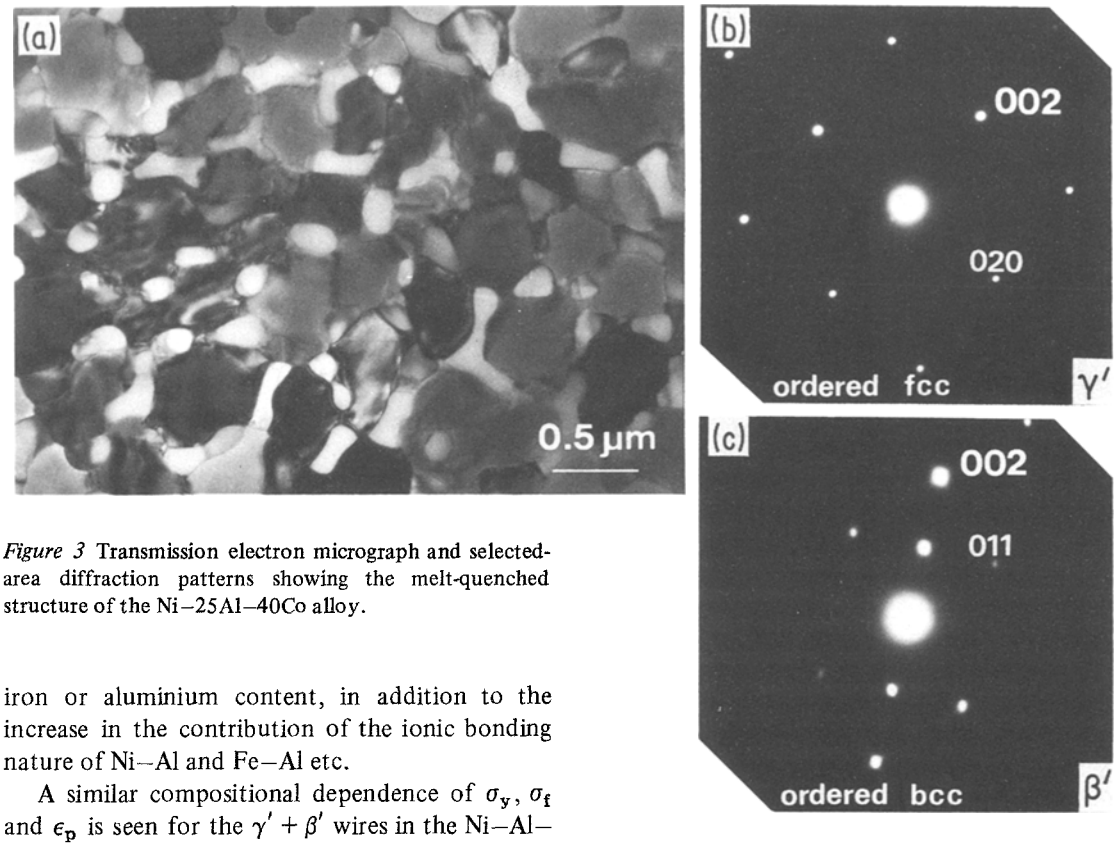

Figure 3 Transmission electron micrograph and selected-area diffraction patterns showing the melt-quenched structure of the Ni–25Al–40Co alloy.

iron or aluminium content, in addition to the increase in the contribution of the ionic bonding nature of Ni–Al and Fe–Al etc.

A similar compositional dependence of σ_y, σ_f and ϵ_p is seen for the $\gamma' + \beta'$ wires in the Ni–Al–Co system. As shown in Figs. 9 and 10, σ_y of Ni–25Al–Co and Ni–Al–40Co alloys tends to increase from 250 to 380 MPa and from 260 to 340 MPa, respectively, with increasing cobalt and aluminium content (i.e. increasing volume ratio of β' against $\gamma' + \beta'$). σ_f increases from 600 to 870 MPa with increasing cobalt content, while an increase in aluminium content results in a decrease in σ_f from 840 to 465 MPa. ϵ_p ($\simeq 5\%$) hardly changes against cobalt content and decreases from 7.0 to 2.5% with increasing aluminium content. Thus, it is strongly emphasized that the melt-quenching technique leads to the β' and $\gamma' + \beta'$ compounds exhibiting an elongation as large as $\sim 5\%$ and $\sim 17\%$, respectively, instead of the extremely brittle nature ($\epsilon_p \lesssim 0.2\%$) of conventionally solidified γ' and β' compounds.

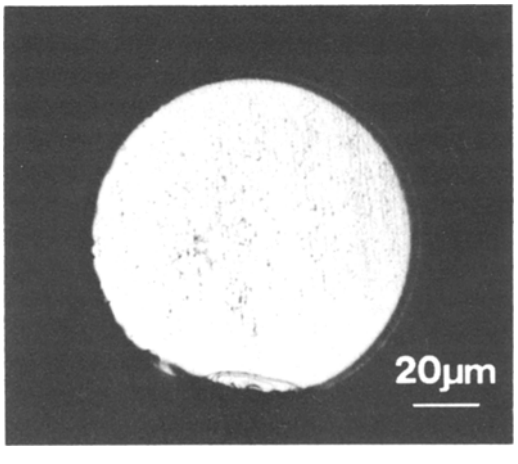

Figure 4 Optical micrograph showing the cross-sectional area of the Ni–20Al–30Fe wire produced by the in-rotating-water spinning method.

3.3. Fracture morphology

Fig. 11 shows the fracture surface morphology of the $\beta' + \gamma'$ wires of (a) Ni–20Al–30Fe, (b) Ni–25Al–40Co, (c) the β' wires of Ni–30Al–20Fe, and (d) Ni–30Al–30Fe systems. The elongation of each wire is about 16.4% for (a), 7.7% for (b), 5.3% for (c) and 0.2% for (d). A typical dimple pattern accompanied by a large reduction in area is seen over the fracture surface of the Ni–20Al–30Fe wire exhibiting a large elongation of about 16.4%. The fracture morphology of the Ni–30Al–20Fe and Ni–25Al–40Co wires exhibiting a relatively large elongation of about 5 to 8%, is composed of the dimple and intergranular fracture patterns, and the Ni–30Al–30Fe wire exhibiting

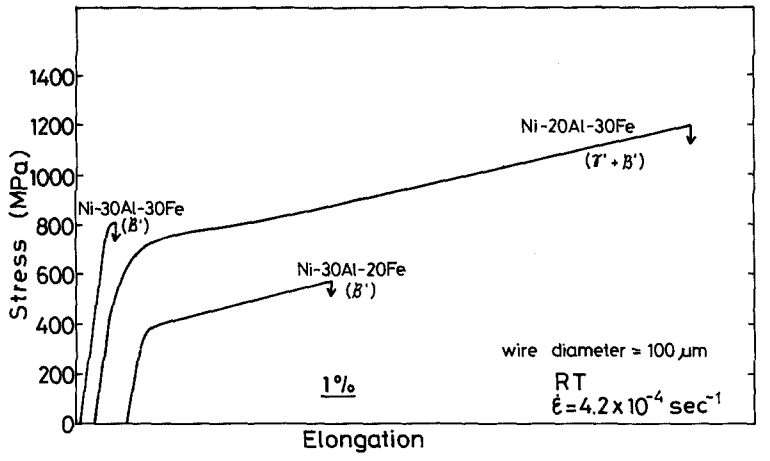

Figure 5 Tensile stress–elongation curves of melt-quenched $\gamma' + \beta'$ and β' compounds in the Ni–Al–Fe system.

an elongation as small as about 0.2%, shows the intergranular and cleavage fracture patterns. Thus, the fracture surface morphology of the $\gamma' + \beta'$ and β' compounds produced by the melt-quenching technique is significantly different from the result showing that the usually cast $\gamma' + \beta'$ and β' compounds occur in intergranular fracture.

3.4. Effect of cold-drawing on mechanical properties

As shown in Figs. 1 and 3, the $\gamma' + \beta'$ wires consist of grains as small as ~ 0.2 μm. Additionally, the duplex phase wires exhibit large elongation accompanied with rather large work-hardening. From these results, it is expected that the $\gamma' + \beta'$ wires would be able to be severely cold-drawn and the values of σ_y and σ_f should significantly be enhanced because of the very fine fibrous structure introduced by cold-drawing. As expected, the $\gamma' + \beta'$

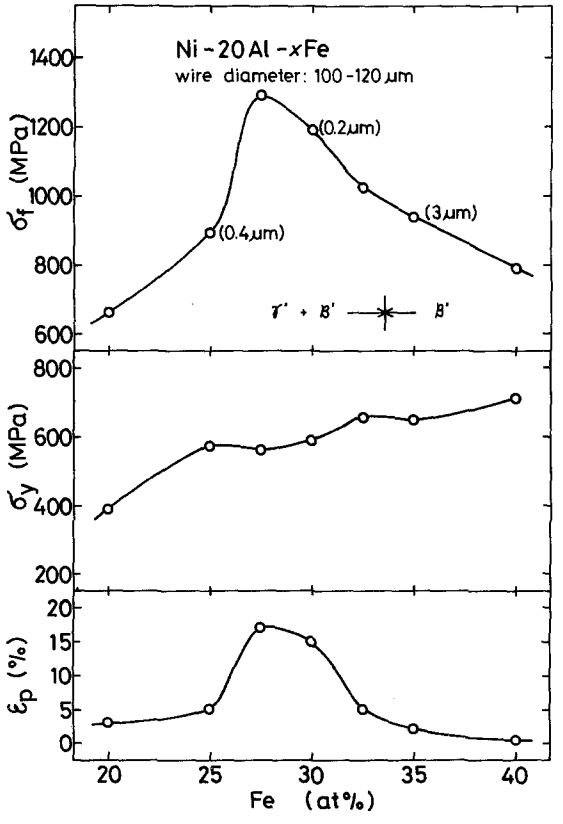

Figure 6 Changes in σ_y, σ_f and ϵ_p of melt-quenched Ni–20Al–Fe alloys with iron content.

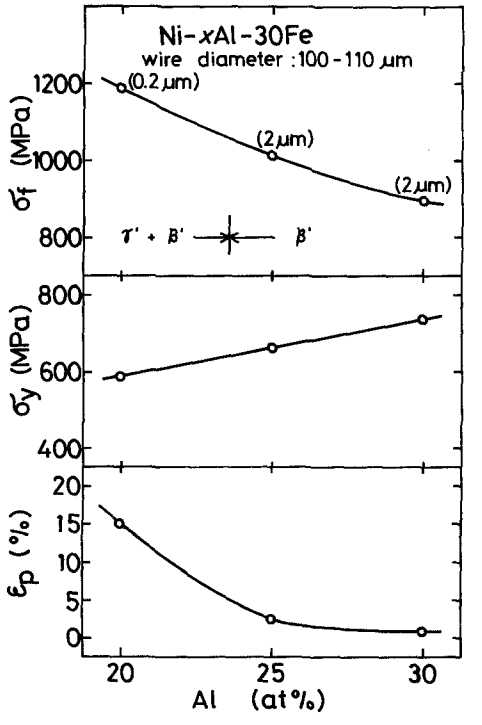

Figure 7 Changes in σ_y, σ_f and ϵ_p of melt-quenched Ni–Al–30Fe alloys with aluminium content.

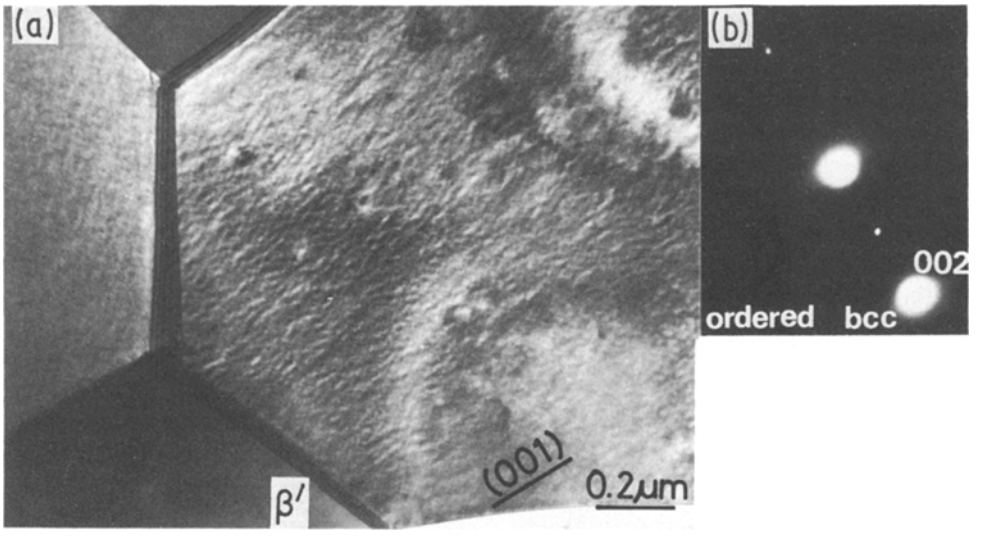

Figure 8 Transmission electron micrograph and selected-area diffraction pattern showing the melt-quenched structure of the Ni–30Al–30Fe alloy.

wires of the melt-quenched Ni–Al–Fe and Ni–Al–Co systems could be cold-drawn from about 100 μm to 30 μm diameter without annealing treatments. σ_y, σ_f and ϵ_p for the cold-drawn Ni–20Al–30Fe and Ni–25Al–30Co wires are plotted as a function of reduction in area in Figs. 12 and 13. σ_y and σ_f are about 600 and 1200 MPa, respectively, for the as-quenched Ni–Al–Fe alloy and about 250 and 600 MPa, respectively, for the as-quenched Ni–Al–Co alloy, increase with increasing reduction in area, and reach about 1850 and 2500 MPa, respectively, for both the alloy wires cold-drawn to about 90% reduction in area. On the other hand, ϵ_p decreases from about 16 to 0.7% for the Ni–Al–Fe wire and from about 7 to 0.2% for the Ni–Al–Co wire with increasing reduction in area. However, the good ductility, shown by the 180° bending, remained unchanged even for the heavily cold-drawn wires

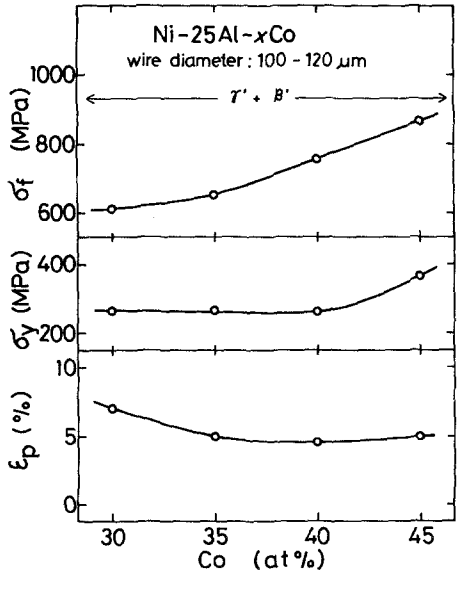

Figure 9 Changes in σ_y, σ_f and ϵ_p of melt-quenched Ni–25Al–Co alloys with cobalt content.

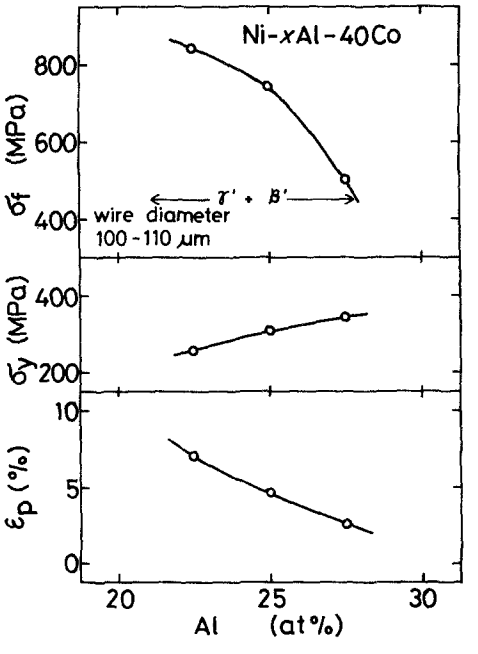

Figure 10 Changes in σ_y, σ_f and ϵ_p of melt-quenched Ni–Al–40Co alloys with aluminium content.

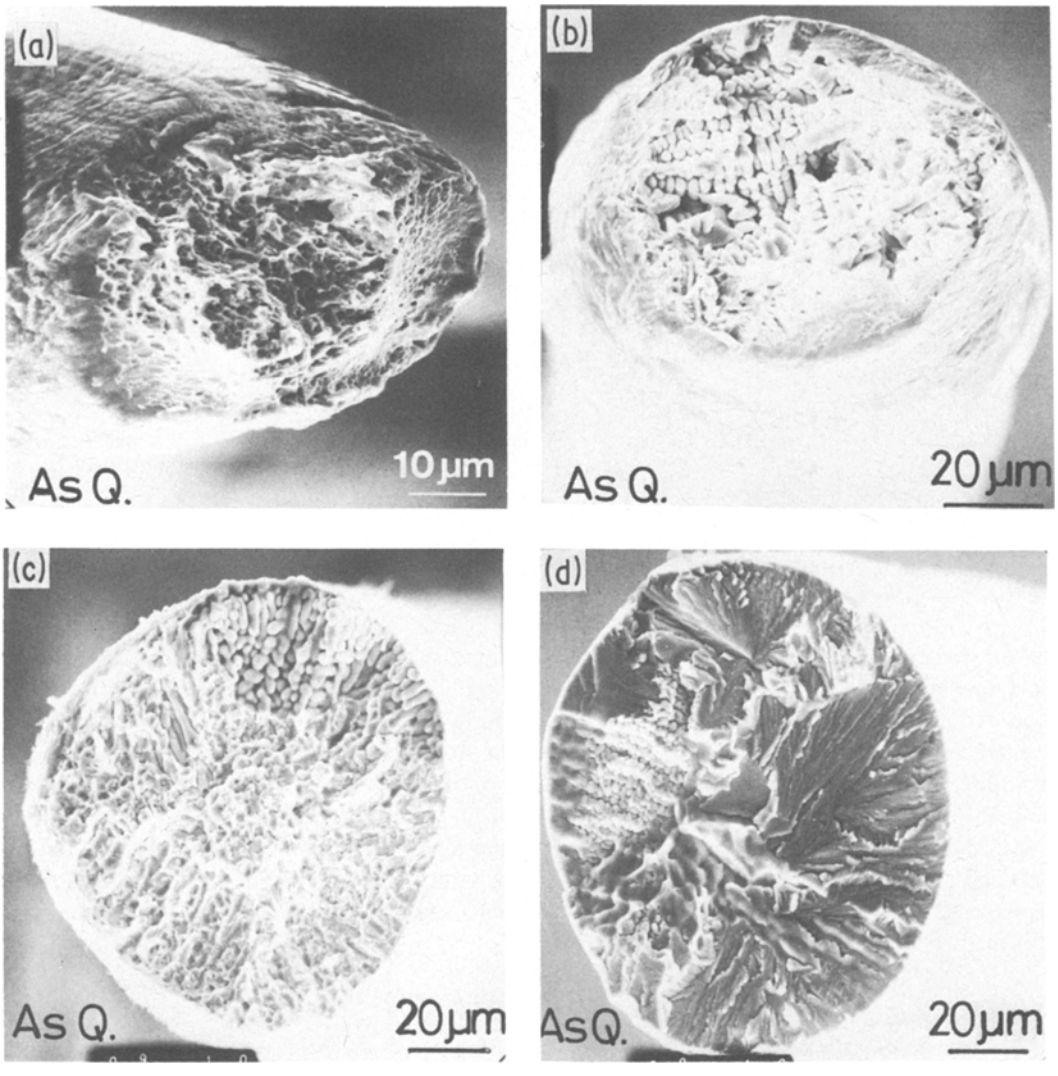

Figure 11 Scanning electron micrographs showing the tensile fracture morphology of melt-quenched $\gamma' + \beta'$ and β' compounds. (a) Ni–20Al–30Fe with $\gamma' + \beta'$ duplex structure, (b) Ni–30Al–20Fe with β' structure, (c) Ni–25Al–40Co with $\gamma' + \beta'$ duplex structure, and (d) Ni–30Al–30Fe with β' structure. (As Q. = as-quenched.)

having a small plastic elongation of about 0.2–0.7%. σ_y and σ_f values attained are about twice as large as the highest values ($\sigma_y \simeq 1270$ MPa and $\sigma_f \simeq 1445$ MPa) [19] of age-hardening type Cu–Be, which is the highest alloy in commercial non-ferrous materials, and are almost equivalent to those of conventional high-strength steels, such as maraging steel and piano wire. Such extremely high values are due mainly to a great work-hardening through the interaction which occurs between a large number of dislocations introduced by severe cold drawing and APB or the phase boundaries between γ' and β' and through the development of the fine fibrous structure of γ' and β' compounds.

4. Discussion

As described in Section 3, the melt-quenched β' and $\gamma' + \beta'$ compound wires in the Ni–Al–Fe and Ni–Al–Co systems exhibited good ductility as well as high strength, in spite of an extremely brittle nature in the usual cast case. The reason for such a remarkable improvement in ductility and strength by melt-quenching their compounds is investigated from the metallographic point of view. Figs. 1 to 3 clearly indicate that melt-quenching results in the refinement of grain size to ~ 0.2 to 4 μm for the γ' and β' phases. Such a refinement of grain size implies a decrease in the size of anti-phase domains (APD) in γ' and β'

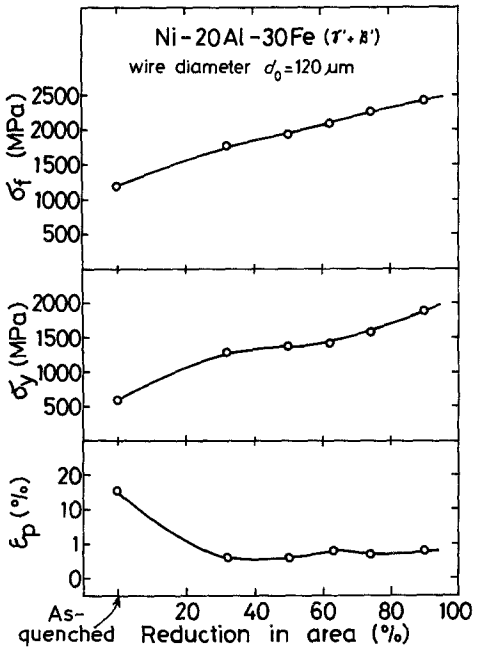

Figure 12 Changes in σ_y, σ_f and ϵ_p of melt-quenched Ni–20Al–30Fe alloy with reduction in area.

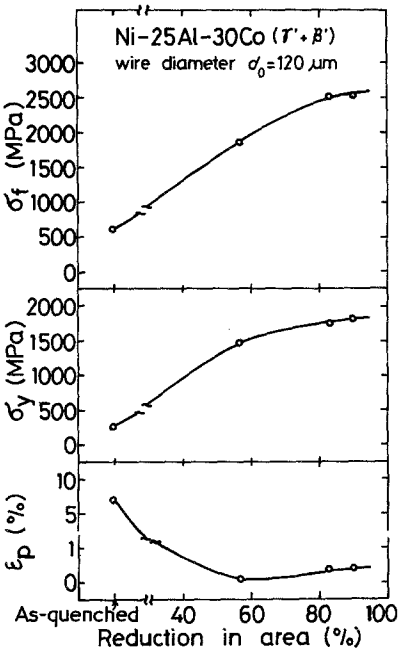

Figure 13 Changes in σ_y, σ_f and ϵ_p of melt-quenched Ni–25Al–30Co alloy with reduction in area.

phases, because each individual grain is occupied with one APD. Additionally, it can be seen in Figs. 1 and 3 that the intensity of the superlattice reflection spots is much weaker for the melt-quenched γ' compound than for the usually cast γ' compound. These results suggest that the degree of ordering in the γ' and β' compounds is weaker in the melt-quenched state. The remarkable increase in the total area of grain boundaries and/or phase boundaries by melt-quenching also results in a significant decrease in the segregated concentration of the solute element per unit area of grain boundaries.

In conclusion, the main structural changes in the β' and $\gamma' + \beta'$ phases achieved by melt-quenching are summarized by the following three points:

1. the refinement of grain size;

2. depression of the development of ordered state; and

3. the suppression of grain-boundary segregation.

The combination of such quenching effects is inferred to be the origin of the improvement in ductility and strength for the melt-quenched β' and $\gamma' + \beta'$ compounds. It was reported in Section 1 that we have succeeded in producing γ' single-phase wires with a high strength combined with large elongation in Ni–Al–X (X = Cr, Mn, Fe, Co or Si) ternary systems [11] and we gave an interpretation of the origin of the remarkable enhancement of strength and ductility. The mechanism by which ductility and strength of the ordered compounds are improved significantly by the melt-quenching technique is thought to be the same for the $\gamma' + \beta'$ and β' wires as well as for the γ' wires.

5. Conclusion

Wires of metastable $\gamma' + \beta'$ duplex or β' single-phase exhibiting high strength and large elongation were produced by the melt-quenching technique in Ni–Al–Fe and Ni–Al–Co systems even though the usually solidified β' and $\gamma' + \beta'$ compounds are extremely brittle. Wire production was carried out using an in-rotating-water spinning apparatus in which the melt was ejected through the orifice of a quartz nozzle into the rotating water layer. The β' wires thus obtained had a nearly circular cross-section, and the maximum wire diameter was about 180 μm. The average grain size was about 0.2 μm for the $\gamma' + \beta'$ duplex phases and about 4 μm for the β' single phase. The yield strength (σ_y), tensile fracture strength (σ_f), and elongation (ϵ_p) of the $\gamma' + \beta'$ wires are about 395 to 660 MPa, 670 to 1285 MPa, and 3.5 to 17%, respectively, for the Ni–Al–Fe system, and about 260 to 365 MPa, 600 to 870 MPa, and 4.0 to 7.0%, respectively, for the Ni–Al–Co system, and those of the β' wires are about 360 to 710 MPa, 560 to 960 MPa, and 0.2 to 5.5%, respectively, for the Ni–Al–Fe

system. The high strengths and large elongation of the melt-quenched β' and $\gamma' + \beta'$ compounds were inferred to be caused by the combination effect of a low degree of ordered state containing a high density of phase boundaries, the suppression of grain-boundary segregation and the refinement of grain size. The $\gamma' + \beta'$ wires could be cold-drawn above 90% reduction in area without annealing treatments. By cold-drawing to about 90% area reduction, σ_y and σ_f increase to about 1850 MPa and 2500 MPa, respectively, for Ni–20Al–30Fe and Ni–25Al–30Co alloys owing to a remarkable work-hardening ability caused by the interaction between a high density of phase boundaries and a large number of dislocations introduced by cold-drawing, and by the development of the two-phase fibrous structure.

References

1. T. MINEMURA, A. INOUE, Y. KOJIMA and T. MASUMOTO, *Met. Trans.* A-11 (1980) 671.
2. A. INOUE, T. IWADACHI, T. MINEMURA and T. MASUMOTO, *Trans. Jap. Inst. Metals* 22 (1981) 197.
3. T. MINEMURA, A. INOUE and T. MASUMOTO, *Trans. Iron Steel Inst. Jap.* 21 (1981) 649.
4. A. INOUE, Y. KOJIMA, T. MINEMURA and T. MASUMOTO, *ibid.* 21 (1981) 656.
5. A. INOUE, T. MINEMURA, A. KITAMURA and T. MASUMOTO, *Met. Trans.* A-12 (1981) 1041.
6. A. INOUE, Y. KOJIMA, T. MINEMURA and T. MASUMOTO, *ibid.* A-13 (1982) 337.
7. T. MINEMURA, A. INOUE, Y. KOJIMA and T. MASUMOTO, *ibid.* A-13 (1982) 337.
8. A. INOUE, H. TOMIOKA, M. HAGIWARA and T. MASUMOTO, *Trans. Jap. Inst. Metals* 23 (1982) 341.
9. A. INOUE, H. TOMIOKA and T. MASUMOTO, *Met. Trans.* A-14 (1983) 2319.
10. A. INOUE, H. TOMIOKA, T. NAOHARA and T. MASUMOTO, *ibid.* to be submitted.
11. A. INOUE, H. TOMIOKA and T. MASUMOTO, *ibid.* A-14 (1983) 1367.
12. M. HIRABAYASHI and H. IWASAKI, "Superlattice and Order-Disorder Transformation" (Japan Institute of Metals, Sendai, 1967) p. 63.
13. R. W. GUARD and J. H. WESTBROOK, *Trans. AIME* 215 (1956) 807.
14. A. J. BRADLEY and A. TAYLOR, *J. Inst. Metals* 66 (1940) 53.
15. J. SCHRAMM, *Z. Metallkde.* 33 (1941) 403.
16. I. OHNAKA, T. FUKUSAKO and T. DAIDO, *J. Jap. Inst. Metals* 45 (1981) 751.
17. T. MASUMOTO, I. OHNAKA, A. INOUE and M. HAGIWARA, *Scripta Metall.* 15 (1981) 293.
18. A. BALL and R. E. SMALLMAN, *Acta Metall.* 14 (1966) 1349.
19. "Metals Databook" (Japan Institute of Metals, Maruzen, Tokyo, 1974) p. 156.

Received 24 October
and accepted 19 December 1983